

Anderson localization through Polyakov loops: lattice evidence and Random matrix model

Falk Bruckmann,¹ Tamás G. Kovács,² and Sebastian Schierenberg¹

¹*Institut für Theoretische Physik, D-93040 Regensburg, Germany*

²*Department of Physics, University of Pécs, H-7624 Pécs, Ifjúság útja 6, Hungary*

We investigate low-lying fermion modes in $SU(2)$ gauge theory at temperatures above the phase transition. Both staggered and overlap spectra reveal transitions from chaotic (random matrix) to integrable (Poissonian) behavior accompanied by an increasing localization of the eigenmodes. We show that the latter are trapped by local Polyakov loop fluctuations. Islands of such “wrong” Polyakov loops can therefore be viewed as defects leading to Anderson localization in gauge theories. We find strong similarities in the spatial profile of these localized staggered and overlap eigenmodes. We discuss possible interpretations of this finding and present a sparse random matrix model that reproduces these features.

I. INTRODUCTION

The vacuum of Quantum Chromodynamics (QCD) is a prominent nonperturbative system, whose strongly interacting nature persists even above the transition to the quark-gluon plasma. To get insight into its mechanism, spectral properties of the QCD Dirac operator are very useful. A nonzero density of eigenvalues at zero gives rise to chiral symmetry breaking via the Banks-Casher formula [1]. Moreover, exact zero modes are related to the topological charge via index theorems.

In recent years, localization properties of the Dirac eigenmodes have attracted attention as they can be used to draw analogies to condensed matter phenomena: concepts like the mobility edge and Anderson localization can be studied in QCD lattice simulations. In this spirit the chiral transition at finite temperature¹ has been conjectured to be an Anderson (metal-insulator) transition.

This goes hand in hand with different random matrix theory (RMT) descriptions of the Dirac spectra. In the low temperature phase, the existence of the chiral condensate connects QCD to chiral perturbation theory and random matrix theory (becoming exact in the epsilon-regime), which explains the statistics of the low lying part of the Dirac spectrum [3].

The spectral gap in the high temperature phase, on the other hand, seems to call for the “soft edge” description of RMT, which, however, could not be supported by lattice data [4–7]. Instead, a transition to independent eigenmodes obeying Poisson statistics has been suggested [8]. A refined analysis by one of us has shown, that the bulk of the spectrum is still delocalized and subject to RMT, while the lowest lying eigenmodes display a transition to localization and Poissonian behavior of the eigenvalues [9, 10]. This effect has been confirmed to be universal in the sense that it does not depend on the resolution of the lattice. Observables, like e.g. the number of local-

ized modes, rather scale with the physical volume. On the other hand, Ref. [11] found that localization is essentially a finite volume artifact. However, they used a different, less restrictive definition of localization and thus their results are not in conflict with the rest of the above cited literature.

In this work we give another crucial ingredient of Anderson localization in QCD, namely we identify the “defects” causing it. We show that at high temperature local Polyakov loop fluctuations trap low-lying modes. The average Polyakov loop as an order parameter of the deconfinement (or center) phase transition approaches 1 with increasing temperature. Locally, however, the Polyakov loop takes on other values, in particular close to other center elements, -1 in the case of gauge group $SU(2)$. The phase transition can actually be viewed as a percolation of the physical sector embracing such islands where the Polyakov loop is close to other center elements [12, 13].

The locations of these Polyakov loop fluctuations (which are similar to Weiss domains in ferromagnetism) are correlated with maxima in the profile of low-lying Dirac modes. We will demonstrate this for eigenmodes of both the overlap and staggered operator. Similarities between the spectrum of the overlap and staggered Dirac operator have already been found in the Schwinger model [14] and also in QCD [15]. Our present study is, however, the first one when similarity of staggered and overlap Dirac eigenmodes is seen in lattice simulations and we consider this an important side result of our study.

The observed localization can be understood via Polyakov loops compensating the twist caused by the antiperiodic boundary conditions in the temporal direction. The corresponding Matsubara frequency is effectively lowered (locally) which results in lower eigenvalues. Actually, our finding has been inspired by a similar localization effect in the spectrum of the gauge-covariant Laplace operator [16]. The Laplacian is the square of the Dirac operator in the free case, so the twist picture applies. Otherwise this operator does not share important chiral features like topological zero modes and condensates.

¹ At zero temperature the situation is not clear due to the continuum limit, see [2] and references therein.

Likewise, our finding is consistent with the existence of a chiral condensate in the Polyakov loop sector close to other center elements [17–24] (also needed for center symmetry breaking [25]), which implies low Dirac eigenvalues in islands of such Polyakov loops.

The connection of these islands to topological excitations like magnetic monopoles is attractive, but in its naive form contradicts the observed topological susceptibility quantitatively, see below.

For the construction of random matrix models valid at high temperature we investigate the distribution of local Polyakov loops and find them to be uncorrelated to a good approximation. Hence, Polyakov loops in fact provide the Poissonian ingredient for the Dirac spectrum. This is built into a novel Anderson-like random matrix model through supplementing it by random matrix entries that represent nearest neighbor hoppings in three-dimensional space. We motivate this model and show, that with a few parameters it reproduces the main features of the Dirac modes: chirality, spectral gap, RMT-Poisson transition and localization (to the analogue of local Polyakov loops).

Our findings are based on quenched lattice simulations with the $SU(2)$ gauge group, we strongly believe that the described phenomena are present in more realistic gauge theories, too.

The paper is organized as follows. In the next section we describe the Dirac spectra at high temperature including the RMT-Poisson (chaotic to integrable) transition and the similarity of the staggered and overlap modes. Sect. III is devoted to the connection between local Polyakov loops and low-lying modes. In Sect. IV thereafter we investigate two possible interpretations of this finding, effective Matsubara frequencies and topological objects. In Section V we introduce and explore our random matrix model and finally Section VI contains our conclusions.

II. DIRAC SPECTRA AT HIGH TEMPERATURE

We analyze quenched $SU(2)$ lattice configurations generated with Wilson action on a $24^3 \cdot 4$ lattice at $\beta = 2.6$ which amounts to a temperature of $2.6T_c$. The average Polyakov loop of 0.37 signals deconfinement (by Polyakov loop we refer to the trace of the products of all temporal links $L(\vec{x}) = 1/2 \cdot \text{Tr} \prod_{x_0=1}^{N_t} U_0(x_0, \vec{x})$ and we selected the physical sector of positive Polyakov loops by hand).

We measured the 256 lowest eigenvalues with positive imaginary parts of the overlap [26, 27] (with parameter $s = 0.4$ cf. [9]) and staggered Dirac operator on 1136 (overlap)/ 3149 (staggered) configurations. For a set of 1102 configurations, we also measured the 12 lowest eigenmodes of both staggered and overlap operator. In all cases the quark mass was set to zero.

The eigenvalues are ordered according to their imaginary parts and the corresponding eigenvalue densities² are plotted in Fig. 1. They display a gap-like behavior with the eigenvalue density starting to differ from zero considerably at $a\lambda \simeq 0.15$ and $a\lambda \simeq 0.5$, respectively. In addition, the overlap operator possesses exact zero modes, which we use to determine the topological charge of the configuration.

To describe the RMT vs. Poissonian behavior of the Dirac spectra we will scan windows in the range of available eigenvalues and measure the level spacing distributions $P(s)$ on unfolded eigenvalues [3], a typical quantity describing the eigenvalue statistics. The Gaussian RMT ensembles provide predictions for it, which also apply to systems with chiral symmetry, depending only on the universality class. For gauge group $SU(2)$ the latter are the Gaussian Orthogonal Ensemble (GOE) for the overlap operator (like for the continuum Dirac operator) and the Gaussian Symplectic Ensemble (GSE) for the staggered operator. The main difference of those $P(s)$ formulae lies in the different repulsion strength of nearby eigenvalues, which results in a linear and quartic behavior of $P(s)$ near $s = 0$, respectively. Independent eigenvalues, on the other hand, lack such a repulsion and the unfolded level spacing is a Poissonian distribution, i.e. $P(s) = \exp(-s)$.

Fig. 2 shows the level spacing distribution of overlap eigenvalues (see [10] for staggered spectra). It clearly reveals that the level spacing agrees with the associated RMT predictions in the bulk and moves towards Poisso-

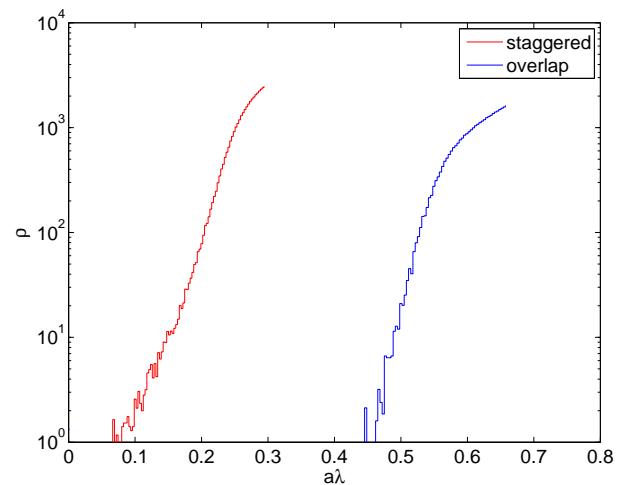


FIG. 1: Logarithm of the spectral density along the imaginary axis for the staggered (red, at smaller λ) and overlap (blue) Dirac operator from the lowest 256 eigenvalues.

² Due to chirality, the nonzero eigenvalues come in pairs of opposite imaginary part and we restrict ourselves to the half with positive imaginary part. In other words, all plots can be extended symmetrically around $\lambda = 0$.

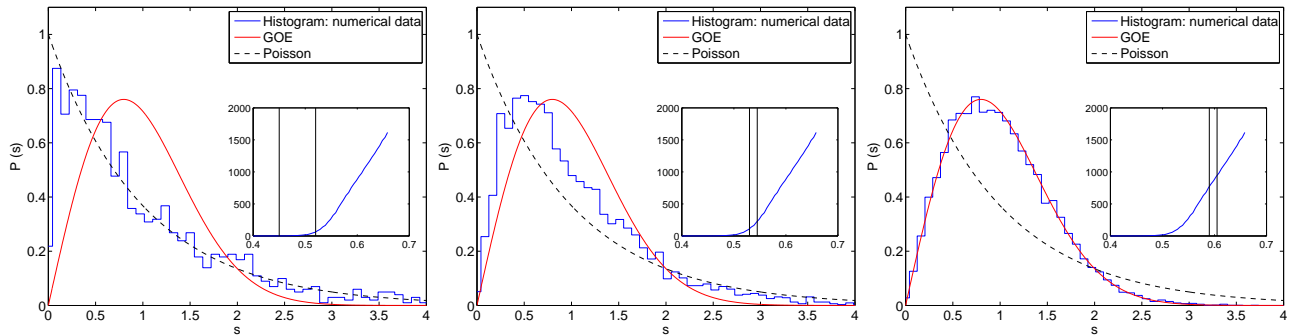


FIG. 2: Spacing distributions of the overlap spectrum in spectral windows indicated by the insets showing the spectral density. The pure RMT (GOE) prediction and the Poissonian distribution are plotted for comparison.

nian when the spectral window is shifted towards lower eigenvalues. To observe such a level *spacing* at least a few independently (Poissonian) distributed eigenvalues are needed on each configuration. Since independent modes occur only at the very low end of the spectrum where the spectral density is low, large enough volumes are required for that. In [9] also the independence of these data of the lattice spacing has been demonstrated for the staggered case.

The properties of the independent and localized modes at the lower ends of the spectra are the main subject of the rest of the paper. We therefore check first, whether the modes of the overlap and the staggered operator see similar physical effects, meaning that their profiles are correlated and localized to similar locations.

First of all we remark that for every overlap zero mode we find a staggered eigenvalue with unusually small value. In the topological sector $Q = 0$, the average smallest eigenvalue is 0.175(1), whereas it is 0.109(3) for $|Q| = 1$ (and 0.098(8)/0.141(6) for $|Q| = 2$, where we have two small eigenvalues). This can also be seen in Fig. 7 bottom.

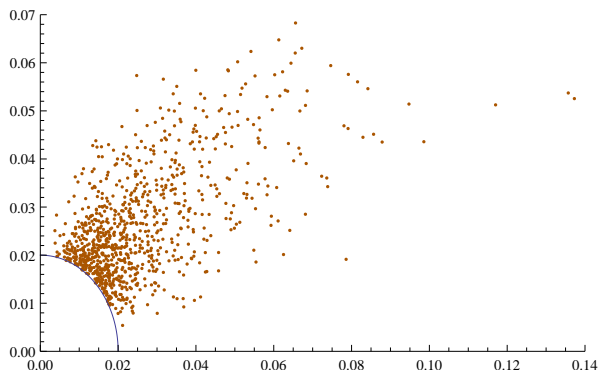


FIG. 3: Scatter plot of staggered (horizontal) vs. overlap (vertical) amplitudes for the lowest modes, $|\psi_1^{\text{st}}(x)|$ vs. $|\psi_1^{\text{ov}}(x)|$, on a $Q = 0$ configuration over the whole lattice. Data points with small amplitudes – as indicated by the circle – have been excluded to avoid overcrowding the plot.

Next, the scatter plot of Fig. 3 gives a strong indication for the correlation of the local mode amplitudes in a typical example configuration, which is further visualized by the two-dimensional profiles in Fig. 4.

In order to quantify the similarity and localization of two modes we propose the following “interlocalization”

$$I := N \sum_x |\psi_m^{\text{ov}}(x)|^2 |\psi_n^{\text{st}}(x)|^2, \quad (1)$$

where N is the number of lattice sites, and $|\psi_m^{\text{ov,st}}(x)|$ is the absolute value (L^2 -norm) of the m th over-

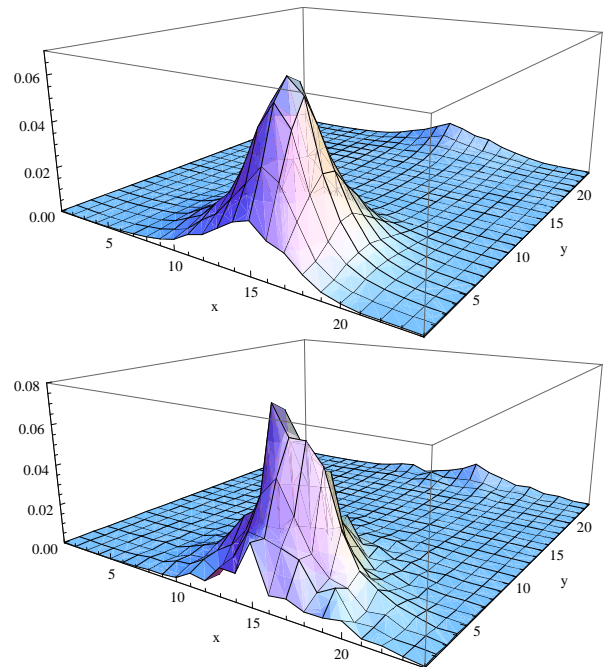


FIG. 4: Profile of the overlap (top) and staggered (bottom) lowest mode of the configuration of Fig. 3, in a lattice plane where the overlap mode takes on its maximum. (The absolute maximum of the staggered mode is separated from the overlap one by $\sqrt{2}$ lattice spacings in the remaining directions.)

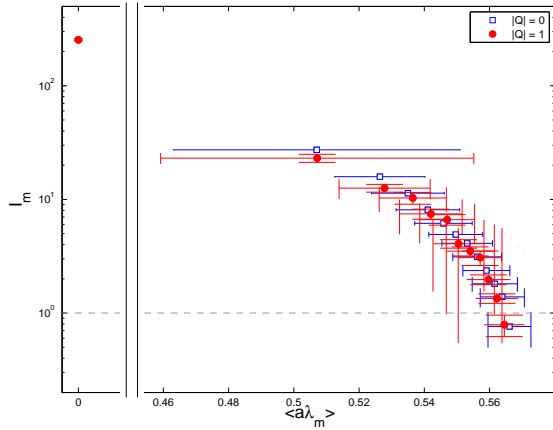


FIG. 5: The interlocalization I , Eq. (1), for matched modes (see text) as a function of the averaged overlap eigenvalue $\langle a\lambda_m \rangle$ (in lattice units), on a logarithmic scale and ensemble averaged. The maximal possible value for I on our lattice is $24^3 \cdot 4 \simeq 5.5 \cdot 10^4$, whereas delocalized modes yield $I \simeq 1$, indicated by the dashed gray line. Horizontal error bars visualize the spreads of the eigenvalues.

lap/staggered eigenmode summed up over gauge – and in the case of overlap also spinor – indices at lattice site x . This is a positive quantity that receives large contributions when both modes are considerably large at some locations. Moreover, for two identical modes it becomes their inverse participation ratio (IPR). The latter is a well-known measure for the localization, taking on a value of N for modes localized on a single point (on the lattice) and 1 for constant modes. In fact, we find $I \simeq 1$ also for two normalized modes with independent Gaussian distributed amplitudes at each site. Only modes that are similar *and* localized generate large values of I .

We utilize I for matching the overlap and staggered modes³. We start by taking the lowest overlap mode and pair it with the staggered mode that has the largest interlocalization with it. Going up in the overlap spectrum we continue this matching procedure in the same way, but use only those staggered modes that have not yet been paired up with a lower overlap mode. In Fig. 5 we plot the interlocalization values for the lowest modes matched in this way as a function of the corresponding overlap eigenvalue λ_m . From this plot it is clear that the zero modes (of the overlap operator, near-zero modes of the staggered operator) are matching close to perfectly. The value of 300 is actually in the same order of magnitude as the IPR of the individual overlap zero modes⁴. Then I drops quickly and after a few modes it reaches the reference value 1 discussed above.

³ In [28] the positions of the highest peaks were used to reveal similarities between overlap and staggered modes.

⁴ The associated low-lying staggered modes have a slightly larger IPR, around 400, presumably because in contrast to the overlap operator the staggered operator is ultralocal.

III. POLYAKOV LOOPS AS DEFECTS/TRAPS

As an appetizer of our main finding we show in Fig. 6 the Polyakov loops (of one example configuration) in the lattice plane, where the lowest overlap and staggered eigenmodes take on their maximum, as shown in Fig. 4. The Polyakov loop is dominated by UV fluctuations at the scale of the lattice spacing as almost every lattice observable. Therefore it is virtually impossible to see any structures in it.

We applied 6 sweeps of APE smearing [29, 30] with $\alpha = 0.55$ to the configuration, which leads to a smoother Polyakov loop landscape. Indeed, an island of Polyakov loop with opposite sign emerges at the location of the maximum of the lowest Dirac mode on the original unsmeared configuration. A similar profile becomes visible after simply averaging the (traced) Polyakov loops with their neighbors.

Let us stress, that the lower panel of Fig. 6 is the only occasion that we present a smeared result. We now return to correlation functions of unsmeared Polyakov loops for the rest of this paper.

To check the correlation of Polyakov loop islands and low Dirac modes in a quantitative way, we define “Polyakov loops as averaged by a particular mode”, i.e. Polyakov loops weighted with the density of a normalized

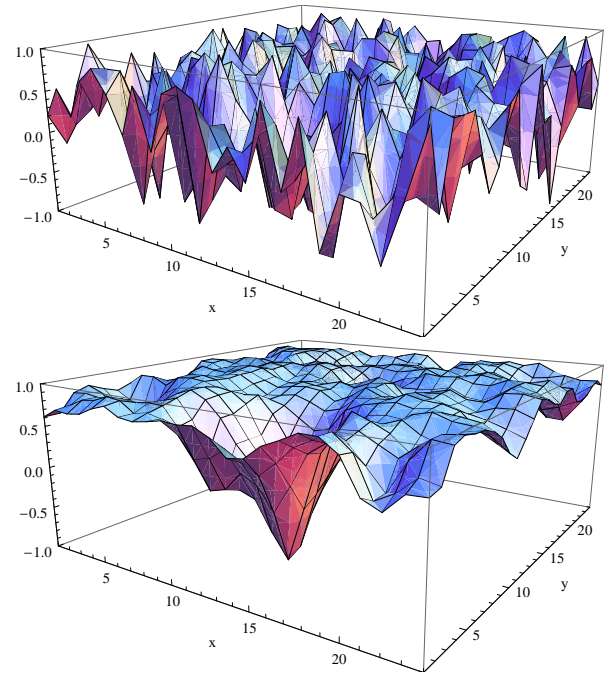


FIG. 6: Profile of the unsmeared (top) and smeared (bottom) Polyakov loop for the same configuration and in the same plane as in Fig. 4. By the naked eye nothing seems particular in this plane for the unsmeared case, whereas the smeared Polyakov loop actually takes its minimum (-0.68, compared to an average smeared Polyakov loop of 0.80) at the hotspot visible in the fermion modes in Fig. 4. (A correlation of the unsmeared Polyakov loop to fermion modes is exposed by virtue of statistical measurements, see text.)

Dirac mode, cf. [16],

$$L_m := \sum_x |\psi_m(x)|^2 L(x). \quad (2)$$

This quantity is restricted to the interval $[-1, 1]$, just like the Polyakov loop L . It is clear that a wave-like mode ψ_m with approximately constant amplitude yields an L_m close to the average Polyakov loop $\sum_x L(x)/V$, whereas a strongly localized mode picks the Polyakov loop in that region. If the latter happens to be an island of “wrong” Polyakov loops, L_m tends to zero or even becomes negative.

Fig. 7 shows the ratio of L_m averaged over different configurations and the average Polyakov loop, both for the low-lying overlap and low-lying staggered modes. The Polyakov loops averaged by the low-lying modes are indeed smaller than on average. Higher modes, on the

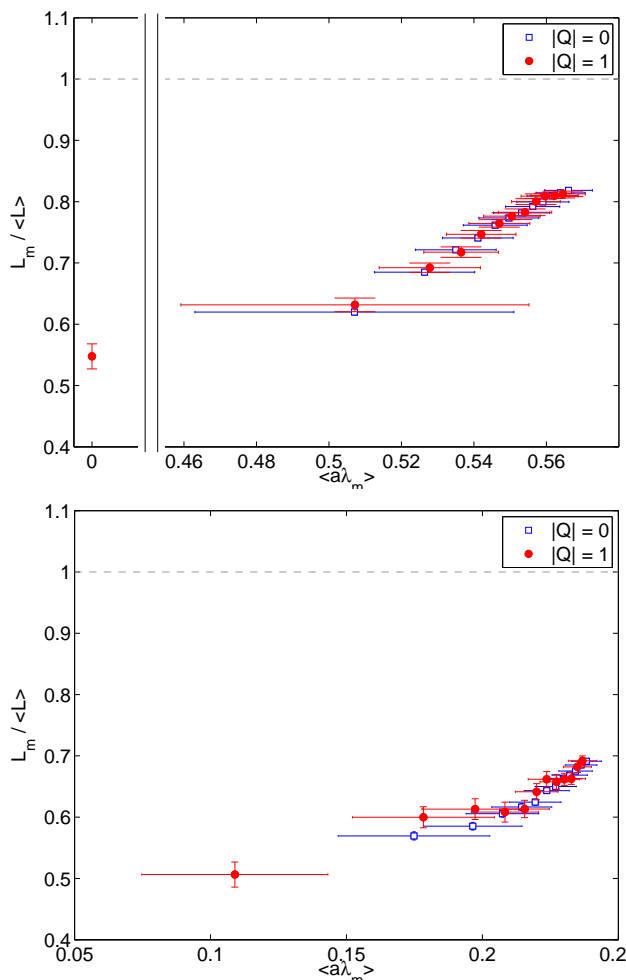


FIG. 7: The ratio of “Polyakov loops as averaged by low-lying modes” L_m , Eq. (2), to the average Polyakov loop for overlap (top) and staggered modes (bottom) as a function of the corresponding averaged eigenvalue $\langle a\lambda_m \rangle$. Horizontal error bars visualize the spreads of the eigenvalues.

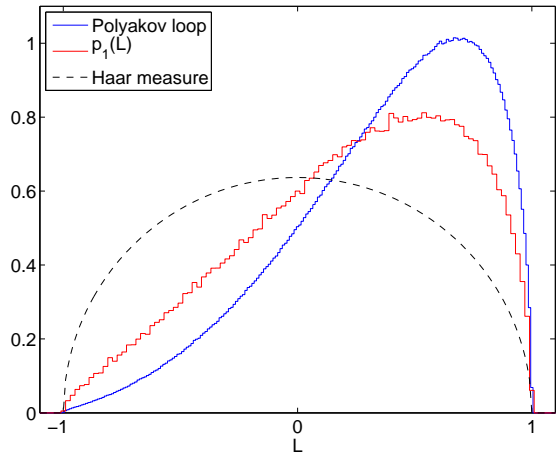


FIG. 8: The “Polyakov loop distribution as seen by the lowest overlap mode”, $p_1(L)$ from Eq. (3), in the $Q = 0$ sector compared to the Polyakov loop distribution and the Haar measure (valid in the low temperature phase).

contrary, tend to see the average Polyakov loop.

The connection between local Polyakov loops and low-lying Dirac modes is confirmed from a slightly different perspective by the following “Polyakov loop distribution as seen by a mode”. For that we weight the probability of Polyakov loops L by the amplitudes of the low-lying modes at those positions x where $L(x) = L$,

$$p_m(L) = \sum_x \delta_\epsilon(L - L(x)) |\psi_m(x)|^2, \quad (3)$$

in continuous notion with some smeared delta-function δ_ϵ (in practice we rescale histograms). The quantity L_m is recovered by the L -expectation value with this probability,

$$L_m = \int dL p_m(L) L, \quad \left(\int dL p_m(L) = 1 \right). \quad (4)$$

Thus the probability p_m visualizes how the global quantity L_m is generated by modifying the distributions of the local Polyakov loops.

In Fig. 8 we show this probability for the lowest modes of the overlap operator, $p_1(L)$, on $Q = 0$ configurations. One can clearly see that low fermion modes enhance low Polyakov loops down to $L \simeq -1$.

IV. INTERPRETATIONS

A. Effective Matsubara frequencies

In a background of constant temporal and vanishing spatial gauge fields the influence of the Polyakov loop on the Dirac spectra is very clear. We first diagonalize the

Polyakov loop introducing its phase φ ,

$$\prod_{x_0=1}^{N_t} U_0(x_0) = \exp(i\varphi \begin{pmatrix} 1 & \\ & -1 \end{pmatrix}), \quad (5)$$

$$L = \cos \varphi \quad \varphi \in [0, \pi]. \quad (6)$$

We gauge it into the last time slice, where it effectively changes the temporal boundary condition.

The lowest modes of the free Dirac operator in the presence of this Polyakov loop are constant in space and plane waves in time, $\exp(ipx_0T)$. The quantum numbers p are governed by a combination of the antiperiodic temporal boundary condition for fermions and the Polyakov loop phase, namely $p = \pi \pm \varphi + 2\pi\mathbb{Z}$, where the different signs emerge from the different color components, see Eq. (5).

The eigenvalues of the free Dirac operator are these numbers multiplied by the temperature. The lowest ones,

$$\lambda_M^{\text{cont.}} = (\pi - \varphi)T, \quad (7)$$

we name *effective Matsubara frequencies*. These hold in the limit $N_t \rightarrow \infty$, whereas on the lattice one has

$$\lambda_M = \frac{1}{a} \sin \left(\frac{\pi - \varphi}{N_t} \right). \quad (8)$$

At high temperatures the Polyakov loop (at fixed lattice spacing) becomes trivial, $L \rightarrow 1$, hence $\varphi \rightarrow 0$ and the Matsubara frequency is $\lambda_M = \frac{1}{a} \sin(\pi/N_t)$. A more realistic estimate is obtained by using the average Polyakov loop at our temperature $\langle L \rangle = 0.37$, from which we obtain the effective Matsubara frequency in lattice units ($T = 1/N_t a$) as

$$\lambda_M a = \sin \left(\frac{\pi - \arccos 0.37}{4} \right) = 0.47, \quad (9)$$

which is the same order of magnitude as the lower end of the bulk of eigenvalues we measured (consistent with the findings of [11]).

The main point of these considerations is that “wrong” Polyakov loops, $L = -1$ with $\varphi = \pi$, would lead to a vanishing effective Matsubara frequency, $\lambda_M = 0$, and thus to the lowest Dirac eigenvalues.

Of course, in realistic configurations one has to take into account that the Polyakov loop varies in space and that nontrivial spatial links are present. Both will change the Dirac eigenvalues away from the free ones. Nonetheless, the tendency that “wrong” Polyakov loops give rise to smaller eigenvalues persists and explains our finding about their pinning nature.

B. Topological objects

Topological excitations of the gauge field and their zero modes are an attractive hypothesis to explain low-lying

Dirac modes in Yang-Mills theory (and QCD). The chiral condensate at zero temperature is thought of as due to instantons of realistic size and density and the first conjecture about the metal-insulator transition at finite temperature was based on instanton ensembles [31, 32].

The natural topological excitations at finite temperature are magnetic monopoles. They appear as selfdual or antiselfdual solutions of the Yang-Mills equations of motion at finite temperature. As they are also electrically charged, they are called dyons. Dyons can be constituents of calorons (finite temperature instantons) [33, 34], but may exist in isolation as well [35].

In gauge group $SU(2)$, there are two dyons (and two antidions) with opposite magnetic charge. One sort of these dyons is characterized by properties that exactly match our findings: the Polyakov loop at their core is -1 and they possess zero modes with the physical antiperiodic boundary conditions [36, 37] (just like the constant configurations discussed above). The other sort has Polyakov loop $+1$ ⁵ and zero modes with periodic boundary conditions.

In dilute ensembles of dyons most of the zero modes should remain low-lying modes. Then the first sort of dyons could explain the localized modes we analyzed, while the second sort could be responsible for low-lying periodic modes. At a positive average Polyakov loop one expects fluctuations to -1 much less frequent than those to $+1$, cf. Fig. 9. Hence the first sort of dyons could give independent low-lying modes, while the second sort could yield a condensate at periodic boundary conditions. This different appearance can be made quantitative by the different fractions of unit topological charge the two dyon sorts have, which are such that the -1 dyons are indeed heavier as they have a larger (classical) action, see [40] for lattice evidence of this picture and [41] for a simple model.

From the relation of magnetic monopoles to both low-lying modes and topological charge a crucial test of this picture is to compare these two quantities at given temperature and volume. Above the finite temperature transition fluctuations of the topological charge decrease sharply. This can be clearly seen by looking at how the topological susceptibility decreases at higher temperatures. As a result, at high temperature, topological objects presumably form a dilute gas of non-interacting objects. From the index of the overlap Dirac operator we have full information about the fluctuations of the *total topological charge*. Assuming that in the dilute gas topological objects are uncorrelated, this can be used to compute the density of topological objects that in turn can be compared to the density of localized Poissonian Dirac eigenmodes.

In Table I we show the probability of different topo-

⁵ Monopoles also appear as defects [38] of the Polyakov gauge [39], where they have $L = -1$ or $L = +1$ by definition.

$ Q $	0	1	0	1	2
\mathcal{P}_Q	0.958(6)	0.042(6)	0.89(1)	0.105(9)	0.009(3)

TABLE I: The probability of different charge sectors in the $16^3 \times 4$ (first two columns) and $24^3 \times 4$ ensemble (last three columns). The probabilities of charge sectors with the same magnitude but opposite sign have been added.

logical sectors extracted from the index of the overlap Dirac operator. From the low occurrence of the topological charge sector ± 1 and in particular of the sector ± 2 it is indeed clear that topological objects form a very dilute gas. In these volumes it very rarely happens that there is more than one topological object on any given configuration. Since we need only an order of magnitude estimate of the density of topological objects we will ignore the probability of two or more objects occurring on any single configuration. In this approximation we can shortcut the calculation of the density of topological objects, and the average number of topological objects per configuration is just given by the probability of the $|Q| = 1$ sector. On our volumes it is between 0.04 and 0.1 which is clearly far too small to account for the few localized Poissonian modes we found on average per configuration.

This comparison rules out models based on uncorrelated gluonic objects that carry both ($O(1)$) topological charge and (antiperiodic) zero modes. However, it does not exclude combinations of topological objects in which the topological charge cancels, like instanton-antiinstanton molecules originally suggested to be present with light dynamical quarks [42] or molecules of dyons called ‘bions’ carrying one near zero mode [43].

V. RANDOM MATRIX MODEL USING THE STAGGERED DIRAC OPERATOR

Transitions between correlated and uncorrelated eigenvalues like the one observed in the lattice data can be described by RMT models in various ways. One of the simplest possible ansätze is to start with a diagonal matrix, whose entries are uncorrelated random numbers, and add a matrix taken from one of the Gaussian ensembles. This model shows the desired transition in between parts of its spectrum with different eigenvalue density, however, the interpolating spacing distributions are different from the ones in the spectrum of the staggered operator [44]. A possible explanation is the sparseness of this operator and the spatial information that is contained in the next-neighbor interactions. In contrast, the full matrices from the Gaussian ensembles blindly connect all diagonal elements with equal strength.

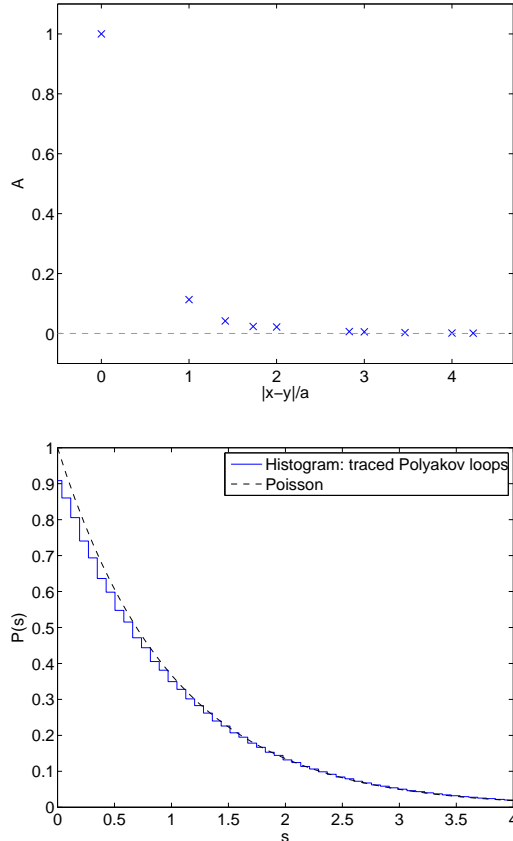


FIG. 9: Independence of local Polyakov loops. Top: the auto-correlation $A := (\langle L(x)L(y) \rangle - \langle L(x) \rangle \langle L(y) \rangle) / (\langle L^2(x) \rangle - \langle L(x) \rangle^2)$ as a function of the lattice distance $|x-y|/a$ (containing the same information as the free energy). Bottom: the level spacing distribution (of the Polyakov loop trace L) compared to the Poisson distribution.

A. Motivation

We construct a better suited random matrix model, based on sparse matrices, in the following. This model can be nicely motivated by our previous findings. Concerning the Polyakov loop, which will be connected to a random potential, three properties are relevant: (i) the distribution of local Polyakov loops extends to negative values and thus small effective Matsubara frequencies, cf. Fig. 8, (ii) Polyakov loops become independent quickly with their distance and therefore (iii) the level spacings of the Polyakov loop trace L – neglecting the spatial information – are distributed according to a Poissonian distribution. The last two properties are depicted in Fig. 9.

Hence the Polyakov loops could provide the Poissonian ingredient for the statistics of the Dirac eigenvalues. To become more concrete, we remind the reader of the defi-

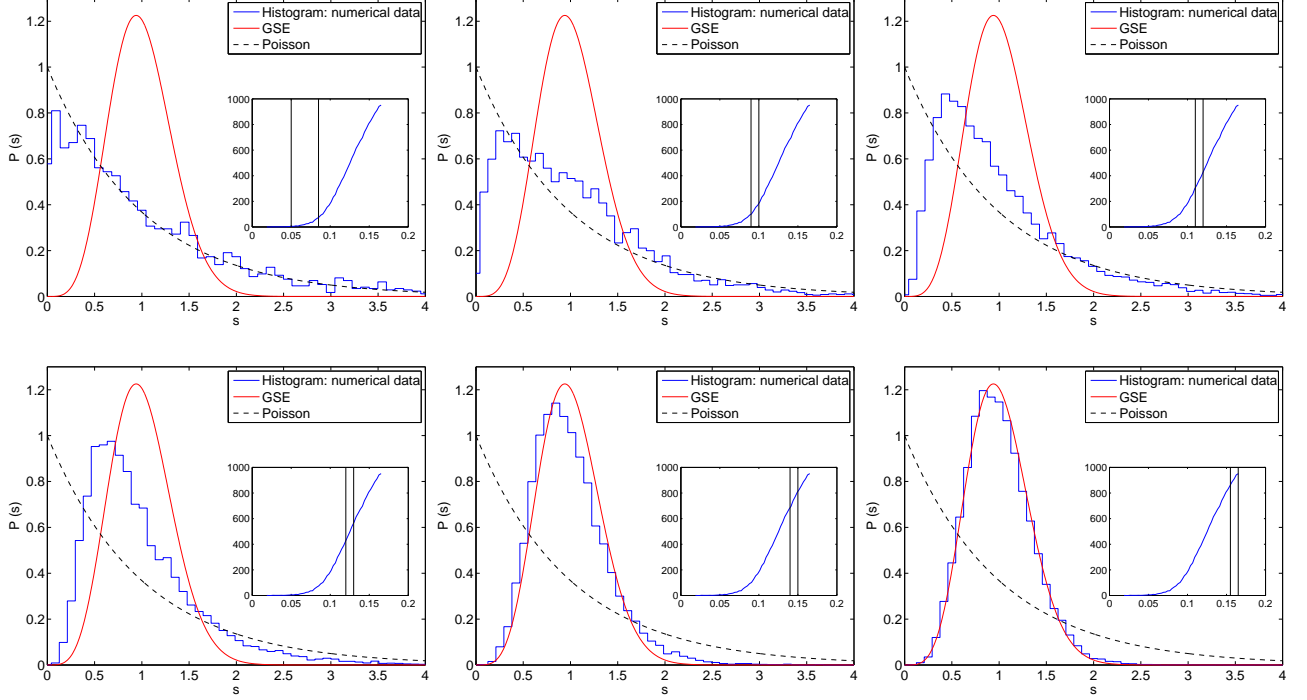


FIG. 10: Spacing distributions in several parts of our RMT spectrum plotted along with the GSE prediction and the Poissonian distribution. The parameters were fixed as discussed in the text. The data was obtained by an ensemble average over 2000 random matrices.

nition of the staggered Dirac operator,

$$D_{xx'} = \frac{1}{2a} \sum_{\mu=1}^4 \eta_{\mu}(x) [\delta_{x+\hat{\mu},x'} U_{\mu}(x) - \delta_{x-\hat{\mu},x'} U_{\mu}^{\dagger}(x')] , \quad (10)$$

with $\eta_{\mu}(x) = (-1)^{\sum_{\nu < \mu} x_{\nu}}$ and $U \in SU(2)$. We split this operator in the temporal and spatial part

$$D = D^{TE} + D^{SP} . \quad (11)$$

D^{TE} contains the hopping terms in the temporal direction, whereas spatial hoppings are included in D^{SP} .

The temporal part has a block-diagonal structure, with one block for each spatial site. We want to approximate each block and thus the whole Dirac operator by restricting it to the subspace of the smallest eigenvalue quadruplet of the temporal operator at each spatial lattice site. The quadruplet consists of two eigenvalue pairs with opposite sign. The plus-minus degeneracy is necessary to conserve chiral symmetry, whereas the exact two-fold degeneracy⁶ has to be kept in order to have the right RMT universality class we find in the $SU(2)$ staggered spectra.

In this basis, the temporal part of the Dirac operator

can be brought in the form

$$D_{\vec{x}\vec{x}}^{TE(n=0)} = \begin{pmatrix} -\theta_{\vec{x}} & 0 & 0 & 0 \\ 0 & -\theta_{\vec{x}} & 0 & 0 \\ 0 & 0 & \theta_{\vec{x}} & 0 \\ 0 & 0 & 0 & \theta_{\vec{x}} \end{pmatrix} , \quad (12)$$

with

$$\theta_{\vec{x}} = \frac{1}{a} \sin \left(\frac{\pi - \varphi_{\vec{x}}}{N_t} \right) , \quad (13)$$

which resemble the effective Matsubara frequencies on the lattice, as given in Eq. (8), however as a function of the local rather than averaged Polyakov loop phase $\varphi_{\vec{x}}$. Therefore, $D^{TE(n=0)}$ is a diagonal matrix with very weakly coupled entries, as argued above. Physically speaking, the temporal part represents a (chiral) random potential.

The spatial part becomes in the restricted basis

$$D_{\vec{x},\vec{x}+\hat{i}}^{SP(n=0)} = \begin{pmatrix} U_{\vec{x},\vec{x}+\hat{i}} & V_{\vec{x},\vec{x}+\hat{i}} \\ V_{\vec{x},\vec{x}+\hat{i}} & U_{\vec{x},\vec{x}+\hat{i}} \end{pmatrix} , \quad (14)$$

where the 2-by-2 matrices U and V can be shown to represent real quaternions.

These have a concrete meaning: U connects eigenvalue pairs of equal sign, and is therefore responsible for the

⁶ In RMT language, this is Kramers degeneracy of the GSE.

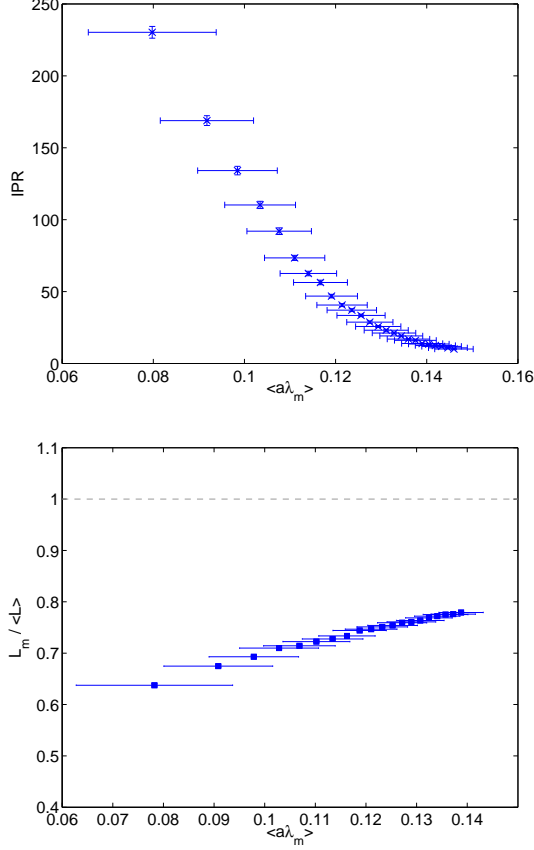


FIG. 11: Top: Inverse participation ratios of the 25 lowest-lying eigenmodes for the RMT model, plotted versus the average eigenvalue of that mode. The data was obtained by an ensemble average over 2000 random matrices. Bottom: diagonal entries “as averaged by the lowest modes” of the RMT model, ϑ_m from Eq. (19), divided by the average diagonal entry, to be compared with Fig. 7. Horizontal error bars visualize the spreads of the eigenvalues.

GSE-like level repulsion between nearest neighbors. V on the other hand generates the gap around zero in the spectrum as it connects eigenvalues of different signs.

B. Explicit construction of the model

We propose a random matrix model based on matrices

$$M = M^{TE} + M^{SP}, \quad (15)$$

that consist of two parts. M^{TE} has the same diagonal structure like $D^{TE(n=0)}$, i.e.

$$M_{\vec{x}\vec{x}}^{TE} = \begin{pmatrix} -\vartheta_{\vec{x}} & 0 & 0 & 0 \\ 0 & -\vartheta_{\vec{x}} & 0 & 0 \\ 0 & 0 & \vartheta_{\vec{x}} & 0 \\ 0 & 0 & 0 & \vartheta_{\vec{x}} \end{pmatrix}, \quad (16)$$

where the diagonal entries

$$\vartheta_{\vec{x}} = t(\pi - \phi_{\vec{x}}) \quad (17)$$

are random numbers constructed with an overall scale t and a random angle $\phi_{\vec{x}} \in [0, \pi]$. These quantities are equivalent to the effective Matsubara frequencies $\theta_{\vec{x}}$ in the continuum, Eq. (7), the temperature T and the angle $\varphi_{\vec{x}}$ of the local Polyakov loop, respectively.

For $\phi_{\vec{x}}$ we have taken the empirical distribution of the angle $\arccos L(\vec{x})$ of local Polyakov loops, by converting the fine histogram in Fig. 8 accordingly. This yields an asymmetric distribution of $\phi_{\vec{x}}$ between 0 and π with a maximum below $\pi/2$ (i.e. at positive Polyakov loop). Its most important feature, however, seems to be the tail towards the “trapping” $\phi_{\vec{x}} \simeq \pi$ (negative Polyakov loop locally), since we have observed that most of the features of the model persist when using the Haar measure $\sin^2 \phi$ as distribution [not shown].

For the spatial part, one first of all needs to fix the periodicity of the underlying space, i.e. an integer N_s such that \vec{x} is identified with $\vec{x} + N_s \hat{i}$, with unit vectors \hat{i} in each of the spatial directions. M^{SP} , like $D^{SP(n=0)}$, has nonvanishing entries only at positions that connect next neighbors in that space. Its blocks

$$M_{\vec{x}, \vec{x}+\hat{i}}^{SP} = \begin{pmatrix} u_{\vec{x}, \vec{x}+\hat{i}} & v_{\vec{x}, \vec{x}+\hat{i}} \\ v_{\vec{x}, \vec{x}+\hat{i}} & u_{\vec{x}, \vec{x}+\hat{i}} \end{pmatrix}, \quad (18)$$

consist of random real quaternions u and v , that are RMT counterparts of U and V from Eq. (14). We have taken them to be Gaussian distributed around zero with their mean deviations σ_u, σ_v as parameters of the model.

By rescaling all the random matrices M it is clear, that only the ratios of the scales t, σ_u and σ_v are relevant parameters. To fix them we have measured the ratio of the average determinants⁷ of the empirical quaternionic hopping terms finding $\langle \det V \rangle / \langle \det U \rangle \approx 1.6^2$ and took this ratio over for the ratio of σ_u^2 / σ_v^2 . The remaining ratio $\sigma_u / t = 0.2$ ($\sigma_v / t = 0.32$) was put in by hand to obtain desired properties of the RMT model, namely a gap at zero and a transition between a Poissonian and a GSE spacing distribution.

The eigenvalue density and spacing distribution of this model are plotted in Fig. 10 for a spatial extent $N_s = 12$ and $t = 1/4$. We observe a similar transition like in the spectrum of the staggered Dirac operator. Another feature that this model shares with the staggered operator is the increasing localization of eigenmodes as the corresponding eigenvalues decrease, quantified by the IPR’s in Fig. 11 top.

In order to measure the correlation of the lowest eigenmodes of this RMT model to the diagonal entries, we

⁷ For real quaternions, the determinant is just the sum over all squared components.

again define the latter “as averaged by a particular mode”

$$\vartheta_m := \sum_{\vec{x}} |\psi_m(\vec{x})|^2 \vartheta_{\vec{x}}. \quad (19)$$

One can see in Fig. 11 bottom, that the low modes are indeed localized to “islands” of low ϑ , which are equivalent to low Polyakov loops. Hence this important effect is shared by our random matrix model, too.

VI. CONCLUSIONS

In the present paper we found a possible explanation for the emergence of localized Poissonian modes at the low end of the high temperature QCD Dirac spectrum. We showed that the localized modes are strongly correlated with large fluctuations of the Polyakov loop. This lowers the effective Matsubara frequencies for modes concentrated there. We argued that the lowest part of the Dirac spectrum consists of this type of eigenmodes. We verified this picture for eigenmodes of both the staggered and the overlap Dirac operator. As a side result we also demonstrated that the spatial structure of the lowest overlap and staggered modes is highly correlated. This shows that different discretizations of the Dirac operator are sensitive to the same type of gauge field fluctuations.

We also looked at the topological charge fluctuations as given by the index of the overlap. Assuming that at high temperature topological objects form a dilute gas and are uncorrelated, we could safely rule them out in creating the localized low modes.

Finally, we proposed a dimensionally reduced random matrix model. It is based on sparse matrices encoding the three dimensional nature of the problem through nearest

neighbor couplings from a lattice Dirac operator. To the best of our knowledge this is an example of a new kind of random matrix models for QCD, where so far only full matrices have been used. Beside chirality and the spectral gap our model reproduces the transition from localized Poissonian to delocalized random matrix type modes observed in the lattice Dirac spectrum as well as the correlation of the localized modes to “islands” of low on site “potential”.

It is instructive to compare the Dirac operator to the Hamiltonian of Anderson type models, see [45, 46] for reviews. In the latter case usually diagonal (on site) disorder is responsible for creating the transition to localized eigenmodes. In the case of the Dirac operator, the on site terms do not seem to be relevant. In fact, in the staggered operator they are exactly zero. However, in our dimensionally reduced three dimensional effective model the non-zero fluctuating on site terms are dynamically generated by fluctuations of the local Matsubara frequency resulting from fluctuations of the Polyakov loop. In this way our dimensionally reduced effective random matrix model is analogous to the Anderson model. It would be interesting to study further how the presence and details of the transition depend on the parameters and matrix size defining the random matrix ensemble.

VII. ACKNOWLEDGEMENTS

We thank helpful discussions to Jacques Bloch, Antonio M. Garcia-Garcia, Ferenc Pittler, Mithat Ünsal and Tilo Wettig. FB and SS are supported by DFG (BR 2872/4-2) and TKG by EU Grant (FP7/2007-2013)/ERC n°208740.

-
- [1] T. Banks and A. Casher, Nucl. Phys. **B169**, 103 (1980).
 - [2] P. de Forcrand, AIP Conf. Proc. **892**, 29 (2007), hep-lat/0611034.
 - [3] J. J. M. Verbaarschot and T. Wettig, Ann. Rev. Nucl. Part. Sci. **50**, 343 (2000), hep-ph/0003017.
 - [4] F. Farchioni, P. de Forcrand, I. Hip, C. B. Lang, and K. Splittorff, Phys. Rev. **D62**, 014503 (2000), hep-lat/9912004.
 - [5] P. H. Damgaard, U. M. Heller, R. Niclasen, and K. Rummukainen, Nucl. Phys. **B583**, 347 (2000), hep-lat/0003021.
 - [6] R. Narayanan, H. Neuberger, Phys. Lett. **B638**, 546 (2006), hep-th/0605173.
 - [7] R. Narayanan, H. Neuberger, Phys. Lett. **B646**, 202 (2007), hep-lat/0612006.
 - [8] A. M. Garcia-Garcia and J. C. Osborn, Phys. Rev. **D75**, 034503 (2007), hep-lat/0611019.
 - [9] T. G. Kovacs, Phys. Rev. Lett. **104**, 031601 (2010), 0906.5373.
 - [10] T. G. Kovacs and F. Pittler, Phys. Rev. Lett. **105**, 192001 (2010), 1006.1205.
 - [11] R. V. Gavai, S. Gupta, and R. Lacaze, Phys. Rev. **D77**, 114506 (2008), 0803.0182.
 - [12] L. G. Yaffe and B. Svetitsky, Phys. Rev. **D26**, 963 (1982).
 - [13] C. Gattringer, Phys. Lett. **B690**, 179 (2010), 1004.2200.
 - [14] S. Dürr, C. Hoelbling, Phys. Rev. **D69**, 034503 (2004), hep-lat/0311002.
 - [15] S. Dürr, C. Hoelbling, U. Wenger, Phys. Rev. **D70**, 094502 (2004), hep-lat/0406027.
 - [16] F. Bruckmann and E.-M. Ilgenfritz, Phys. Rev. **D72**, 114502 (2005), hep-lat/0509020.
 - [17] S. Chandrasekharan and N. H. Christ, Nucl. Phys. Proc. Suppl. **47**, 527 (1996), hep-lat/9509095.
 - [18] M. A. Stephanov, Phys. Lett. B **375**, 249 (1996), hep-lat/9601001.
 - [19] P. N. Meisinger and M. C. Ogilvie, Phys. Lett. B **379**, 163 (1996), hep-lat/9512011.
 - [20] S. Chandrasekharan and S. z. Huang, Phys. Rev. D **53**, 5100 (1996), hep-ph/9512323.
 - [21] C. Gattringer, P. E. L. Rakow, A. Schäfer and W. Söldner, Phys. Rev. D **66**, 054502 (2002), hep-lat/0202009.

- [22] C. Gattringer, S. Schaefer, Nucl. Phys. **B654**, 30 (2003), hep-lat/0212029.
- [23] V. G. Bornyakov, E. V. Lushevskaya, S. M. Morozov, M. I. Polikarpov, E. -M. Ilgenfritz, M. Müller-Preussker, Phys. Rev. **D79**, 054505 (2009), 0807.1980.
- [24] T. G. Kovacs, PoS **LATTICE2008**, 198 (2008), 0810.4763.
- [25] E. Bilgici, F. Bruckmann, C. Gattringer, and C. Hagen, Phys. Rev. **D77**, 094007 (2008), 0801.4051.
- [26] H. Neuberger, Phys. Lett. **B417**, 141 (1998), hep-lat/9707022.
- [27] H. Neuberger, Phys. Lett. **B427**, 353 (1998), hep-lat/9801031].
- [28] R. Höllwieser, “Center Vortices and Chiral Symmetry Breaking”, PhD Thesis, Vienna University of Technology (2009), <http://media.obvsg.at/AC05039334>.
- [29] APE, M. Albanese *et al.*, Phys. Lett. **B192**, 163 (1987).
- [30] M. Falcioni, M. L. Paciello, G. Parisi, and B. Taglienti, Nucl. Phys. **B251**, 624 (1985).
- [31] D. Diakonov, V. Y. Petrov, Phys. Lett. **B147**, 351 (1984).
- [32] A. M. Garcia-Garcia, J. C. Osborn, Nucl. Phys. **A770**, 141 (2006), hep-lat/0512025.
- [33] T. C. Kraan and P. van Baal, Nucl. Phys. **B533**, 627 (1998), hep-th/9805168.
- [34] K.-M. Lee and C.-h. Lu, Phys. Rev. **D58**, 025011 (1998), hep-th/9802108.
- [35] D. J. Gross, R. D. Pisarski, and L. G. Yaffe, Rev. Mod. Phys. **53**, 43 (1981).
- [36] C. Callias, Commun. Math. Phys. **62**, 213 (1978).
- [37] T. M. W. Nye and M. A. Singer, J. Funct. Anal. **177**, 203 (2000), math/0009144.
- [38] G. 't Hooft, Nucl. Phys. **B190**, 455 (1981).
- [39] N. Weiss, Phys. Rev. **D24**, 475 (1981).
- [40] V. G. Bornyakov, E. -M. Ilgenfritz, B. V. Martemyanov, M. Müller-Preussker, Phys. Rev. **D79**, 034506 (2009), 0809.2142.
- [41] F. Bruckmann, PoS **CONFINEMENT8**, 179 (2008), 0901.0987.
- [42] E. -M. Ilgenfritz, E. V. Shuryak, Phys. Lett. **B325**, 263 (1994), hep-ph/9401285.
- [43] M. Ünsal, Phys. Rev. **D80**, 065001 (2009), 0709.3269.
- [44] S. Schierenberg, F. Bruckmann and T. Wettig, in preparation.
- [45] P. A. Lee and T. V. Ramakrishnan, Rev. Mod. Phys. **57**, 287 (1985).
- [46] F. Evers, A. D. Mirlin, Rev. Mod. Phys. **80**, 1355-1417 (2008).